Analysis of Defocused Image Data for 3D Shape Recovery using a Regularization Technique

Murali Subbarao and Yen-Fu Liu
murali@sbee.sunysb.edu , yfliu@sbee.sunysb.edu
Dept. of Electrical Engineering, State University of New York
Stony Brook, New York 11794-2350, USA

ABSTRACT

The reconstruction of three-dimensional (3D) information from defocused image data is formulated as an inverse-problem that is solved through a regularization technique. The technique is based on modeling the sensing of defocused images in a camera system using a three-dimensional (3D) Point Spread Function (PSF). Many images are acquired at different levels of defocus. The difference (mean-square error) between this acquired image data and the estimated image data corresponding to an initial solution for 3D shape is minimized. The initial solution for 3D shape is obtained from a focus and defocus analysis approach. A regularization approach that uses a smoothness constraint is proposed to improve this initial solution iteratively. The performance of this approach is compared with two other approaches: (i) gradient descent based on planar surface patch approximation, and (ii) a local error minimization based on a limited search. We exploit some constraints such as the positivity of image brightness unique to this problem in the optimization procedure. Our experiments show that the regularization approach performs better than the other two and that high accuracy is attainable with relatively moderate computation. Experimental results are demonstrated for geometric optics model of 3D PSF on simulated image data.

Key words: focus and defocus analysis, optimization, inverse problem, 3D shape measurement, regularization.

1 Introduction

A new approach was proposed recently by us[7] for highly accurate reconstruction of three-dimensional (3D) shape and focused image of an object from a sequence of noisy defocused images. This approach unified the two approaches– *image focus analysis* (IFA) and *image defocus analysis* (IDA) – which had been treated separately in the research literature. In the new approach named Unified Focus and Defocus Analysis (UFDA), high accuracy was attained at the cost of increased data acquisition and computation. UFDA was based on modeling the sensing of defocused images in a camera system. A number of images were acquired at different levels of defocus. The resulting data was treated as a function sampled in the 3D space (d, x, y) where x and y were the image spatial coordinates and d was a parameter representing the level of defocus. The concept of a "Three-Dimensional Point Spread Function" (3D PSF) in the (d, x, y) space was introduced. The problem of 3D shape and focused image reconstruction was formulated as an optimization problem where the difference (mean-square error) between the observed image

data and the estimated image data was minimized. The estimated image data was obtained from the image sensing model and the current best known solutions to the 3D shape and focused image. An initial estimation to the solutions was obtained through traditional IFA[6] methods. This solution was improved iteratively by a *gradient descent* approach. This approach reduced the errors in shape and focused image introduced by the image-overlap problem and the non-smoothness of the object's 3D shape. Experimental results were presented to show that the new method yielded improved accuracy.

In this paper we extend our earlier work[7] by proposing a regularization technique to recover focused image and 3D depth-map of scenes. This approach provides substantial improvement in performance in comparison with the gradient descent approach used earlier by us for optimization. The problem of 3D shape and focused image recovery from defocused image data is formulated as an ill-posed inverse optics problem. The definition of a well-posed problem (by Hadamard) is that its solution exists, is unique, and depends continuously on the initial data. In the inverse optics problem considered here, presence of noise in defocused image data and effects of defocusing at borders makes the solution non-existent. Even if noise were absent, the solution will not be unique in those image regions where there is lack of sufficient image contrast. Many ill-posed inverse problems in vision have been solved using the regularization approach so far.[8,9] A matrix based regularization technique was used by Ens[2] for image defocus analysis. This paper presents the application of regularization to UFDA.

The cost functional to be minimized in our approach is a weighted sum of a similarity functional E_i and a stabilizing functional E_s, given by $E_i + \lambda \cdot E_s$. E_i is the difference between the observed image data and estimated image data computed based on an initial solution for depth-map and focused image. E_s is a smoothness constraint based on the Laplacian squared of a local blur parameter, and λ is the regularization parameter. Our choice of the smoothness term based on the Laplacian squared of the blur parameter instead of surface curvature simplifies the derivation of the Euler-Lagrange equation. It also ensures the smoothness of surface structure. Three important constraints are used in minimizing the cost functional. They are– positivity of image brightness and depth, and a local error-control constraint. The first two capture physical reality and restrict the space of possible solutions. The last prevents overshoots and helps in fast convergence of the solution during iteration.

The performance of the regularization approach was compared with that of two other approaches. One is a gradient descent type approach and the other is a local search approach. The regularization approach performed better than the other two approaches in our experiments.

2 Image Formation Model

The image formation model developed by us recently[7] for the case of paraxial geometric optics model is used here. Some relevant parts of this model is summarized in this section. The image coordinates of a point light source is denoted by (x', y') and the image coordinates of a point where the brightness is measured is denoted by (x, y). The camera parameters are (see Fig. 1) $\mathbf{e} = (D, f, s)$ where D is the diameter of camera aperture, f is the focal length of the lens, and s

is the distance between the lens and the image detector. d' is the *blur parameter* of a point light source at distance u' from the camera. It represents the normalized blur circle diameter of the point light source. d is the blur parameter of a fictitious point light source at a known reference distance u. One convenient choice for u is infinity. $u'(x', y')$ denotes the distance or depth of a point source at image coordinates (x', y'). This function represents the depth-map of the 3D scene. The blur parameters are related to the camera parameters and object distance by

$$d \;=\; D\left(\frac{1}{f} - \frac{1}{s} - \frac{1}{u}\right), \quad d' \;=\; D\left(\frac{1}{f} - \frac{1}{s} - \frac{1}{u'}\right), \quad \text{and} \quad d' \;=\; d + D\left(\frac{1}{u} - \frac{1}{u'}\right). \tag{1}$$

The focused image of a scene is denoted by $F(x', y')$ and is defined[4] as the image energy incident on the camera aperture from a point source at image coordinates (x', y'). The image brightness (incident light energy) for a magnification normalized image is denoted by $g(d, x, y)$. d is allowed to change by changing s or/and f while D and u are kept constant. The image of a unit point light source is denoted by $h(d, x, y)$ (see Fig. 2) and it is the three-dimensional point spread function (PSF) of the camera. In this case, the following relation has been derived[7]:

$$g(d, x, y) \;=\; \int_{-\infty}^{\infty}\int_{-\infty}^{\infty}\int_{-\infty}^{\infty} F'(d', x', y')\; h(d - d', x - x', y - y')\; dx'\; dy'\; dd', \tag{2}$$

where

$$F'(d', x', y') = \begin{cases} F(x', y') & \text{if } d' = 0 \text{ or } d = -D\left(\frac{1}{u} - \frac{1}{u'}\right) \text{ and} \\ 0 & \text{otherwise.} \end{cases} \tag{3}$$

Eq. 2 is a 3D convolution expression. Our choice of parameterization of the PSF in terms of the normalized blur circle diameter facilitates the derivation of the convolution expression. Other choices (that are not linearly related to the blur circle diameter) will not lead to the derivation of the convolution expression. In particular, parameterising in terms of s or f directly will not lead to the convolution expression.

The condition

$$d'(s, f, u'(x', y')) = 0 \;\text{ or }\; D\left(\frac{1}{f} - \frac{1}{s} - \frac{1}{u'}\right) \;=\; 0 \tag{4}$$

in Eq. 3 specifies a hyper-surface in the (s, f, u') space. In the (d, x, y) space this surface defines the Focused Image Surface (FIS) of the scene. FIS is denoted by $d_F(x, y)$ and is given by

$$d \;=\; d_F(x, y) = -D\left(\frac{1}{u} - \frac{1}{u'(x, y)}\right) \tag{5}$$

The brightness distribution on this surface will be the focused image[6] $F(x, y)$.

Recording a sequence of images by changing the camera parameters (which results in changing d) is treated as sampling the function $g(d, x, y)$. The sampling period ϵ along the d dimension should be roughly the same as in the (x, y) dimension (i.e. one pixel). The sampling period could be larger than this (ϵ), but choosing it smaller would increase redundancy between two successive image frames.

Given a sequence of images obtained by sampling $g(d, x, y)$, the problem is to find the focused image $F(x', y')$ and the FIS $d_F(x', y')$ defined by Eq. 5. The depth-map $u'(x', y')$ can be determined from FIS using Eq. 5. This problem was formulated as an optimization problem by us earlier[7] and solved using a gradient-descent approach. In this paper, this problem will be solved using a regularization approach.

3 A Regularization Approach to UFDA

The observed defocused image data is denoted by $g_o(d, x, y)$. It can be thought of as an image volume in the (d, x, y) space. The focused image of the scene will be denoted by $F_o(x', y')$ and the FIS of the scene will be denoted by $d_o(x', y')$. The observed image data is related to the focused image and FIS by Eqs. 2, 3. Given an initial estimate of the solution for focused image to be $F_e(x', y')$ and for FIS to be $d_e(x', y')$, the estimated image data $g_e(d, x, y)$ corresponding to the estimated solution can be computed using Eqs. 2,3. Now we can define the similarity functional E_i as

$$E_i \;=\; \int_{-\infty}^{\infty}\int_{-\infty}^{\infty}\int_{-\infty}^{\infty}(g_o(d,x,y) - g_e(d,x,y))^2 \; dx \; dy \; dd \tag{6}$$

The similarity functional is a quadratic error term that represents the mean-square difference between the observed and estimated image data.

We formulate the stabilizing functional E_s as a function of Laplacian square of the estimated FIS $d_e(x', y')$:

$$E_s = \int_{-\infty}^{\infty}\int_{-\infty}^{\infty}(\bigtriangledown^2 d_e(x,y))^2 \; dx \; dy \tag{7}$$

The stabilizing term reflects the physical property of the 3D scene that surfaces are usually smooth. Our choice of the stabilizing term based on the FIS expressed in terms of the blur parameter $d_e(x', y')$ instead of surface curvature simplifies the derivation of the Euler-Lagrange equation. In addition, it offers computational advantages in the UFDA framework.

The cost functional E to be minimized is obtained by combining the similarity functional E_i and the stabilizing functional E_s as

$$E = E_i + \lambda E_s \tag{8}$$

The regularization parameter λ is a weighting factor which controls the closeness of the solution to the data with the degree of regularization. This formulation transforms the ill-posed problem into a well-posed problem.

The solution to the above minimization problem is subjected to additional constraints – positivity of depth and image brightness (for 8 bits/pixel grey-level):

$$0 \;\leq\; u'_e(x', y') \;\;,\;\; \text{and} \;\; 0 \;\leq\; g_e(d, x, y) \;\leq\; 255. \tag{9}$$

Another constraint which was found to be useful is a local error-control constraint. We require that a measure of local error decrease from one iteration to the next. If this is not satisfied, then the solution is not updated in the current iteration. However, it may be upated in the subsequent iterations. This is expressed by

$$e_i^n(x, y) \;\leq e_i^{n-1}(x, y) \tag{10}$$

where n denotes the iteration number and

$$e_i(x,y) \;=\; \int_{-\infty}^{\infty}(g_o(d,x,y)-g_e(d,x,y))^2\;dd \tag{11}$$

The local error-control constraint is used to constrain the solution when the regularization process overestimates or underestimates the solution. This situation arises when the difference between the estimated and observed image data change dramatically from point to point.

According to calculus of variations,[1,3,9] minimizing the functional Eq. (8) is equivalent to solving the associated Euler-Lagrange equation. In order to derive the desired Euler-Lagrange equation, we need to first express E in Eq. (8) more explicitly in terms of the dependent variables and functions. This is made possible by reexpressing the image formation equations 2, 3 in an unusual way. We define a new function $F_e''(d',x',y') = F_e(x',y')$ where $F_e(x',y')$ is the estimated focused image. Note that F_e'' is constant with respect to d'. The structure of the estimated FIS in the (d',x',y') space is specified by $\delta(d'-d_e(x',y'),x',y')$ where $\delta(\cdot)$ is the Dirac delta function. Now the estimated image data $g_e(d,x,y)$ can be expressed as:

$$g_e(d,x,y) \;=\; \int_{-\infty}^{\infty}\int_{-\infty}^{\infty}\int_{-\infty}^{\infty}F_e''(d',x',y')\cdot\delta(d'-d_e(x',y'),x',y')\cdot\;h(d-d',x-x',y-y')\;dx'\;dy'\;dd' \tag{12}$$

Now, by the sifting property[10] of the $\delta(\cdot)$ function, the above equation becomes

$$g_e(d,x,y) \;=\; \int_{-\infty}^{\infty}\int_{-\infty}^{\infty}F_e''(d_e(x,y),x',y')\cdot\;h(d-d_e(x,y),x-x',y-y')\;dx'\;dy'. \tag{13}$$

In the above equation, unlike Eq. 2, integration with respect to d' does not appear. Since the focused image is located only at $d_e(x,y)$, the above equation can be written as

$$g_e(d,x,y) \;=\; \int_{-\infty}^{\infty}\int_{-\infty}^{\infty}F_e(x',y')\cdot\;h(d-d_e(x,y),x-x',y-y')\;dx'\;dy'. \tag{14}$$

Derivation of the above equation which does not involve integration with respect to d' facilitates derivation of the Euler-Lagrange equations for optimization.

Now the functional E can be expressed as

$$E=\int_{-\infty}^{\infty}\int_{-\infty}^{\infty}\mathcal{F}(d_e,\bigtriangledown^2 d_e(x,y))\;dx\;dy \tag{15}$$

where

$$\mathcal{F}(d_e,\bigtriangledown^2 d_e(x,y)) \;=\; \int_{-\infty}^{\infty}(g_o-\int_{-\infty}^{\infty}\int_{-\infty}^{\infty}F(x',y')\cdot\;h(d-d_e(x,y),x-x',y-y')\;dx'\;dy')^2\;dd+ \tag{16}$$
$$\lambda\cdot(\bigtriangledown^2 d_e(x,y))^2$$

Hence, the necessary condition to minimize E is the following Euler-Lagrange equation[1]:

$$\mathcal{F}_{d_e}+\frac{\partial^2}{\partial x^2}\mathcal{F}_{d_{exx}}+\frac{\partial^2}{\partial y^2}\mathcal{F}_{d_{eyy}} \;=\; 0 \tag{17}$$

where $\mathcal{F}_{d_e}$, $\mathcal{F}_{d_{exx}}$ and $\mathcal{F}_{d_{eyy}}$ are partial derivatives of $\mathcal{F}$ with respect to d_e, d_{exx} and d_{eyy}. Here d_{exx} and d_{eyy} are the second order partial derivatives of d_e with respect to x and y. The derivation of the Euler-Lagrange equation is not included in this paper due to space limitation.

From Eq. 16 we obtain

$$\mathcal{F}_{d_e} = \frac{\partial}{\partial d_e}\{\int_{-\infty}^{\infty}(g_o - g_e)^2 dd\} \text{ , and } \frac{\partial^2}{\partial x^2}\mathcal{F}_{d_{exx}} + \frac{\partial^2}{\partial y^2}\mathcal{F}_{d_{eyy}} = 2\lambda \cdot \bigtriangledown^2(\bigtriangledown^2 d_e) \tag{18}$$

Therefore the Euler-Lagrange equation becomes

$$\frac{\partial}{\partial d_e}\{\int_{-\infty}^{\infty}(g_o - g_e)^2 dd\} + 2\lambda \cdot \bigtriangledown^2(\bigtriangledown^2 d_e) = 0 \tag{19}$$

The results in this section so far in terms of continuous functions can be easily extended to the case of discrete sampled functions. Therefore we do not present explicitly the discrete domain equations in order to be concise. In the subsequent parts of this paper, sometimes we refer to the continuous domain equations as if they were discrete domain equations. The context should make our intention clear.

The discrete version of Eq.(19) is obtained by the following procedure. First, the discrete version of Laplacian of Laplacian of blur parameter term $\bigtriangledown^2(\bigtriangledown^2 d_e)$ is expressed in the form[3] $\kappa \cdot (d_{j,k} - \overline{d}_{j,k})$ where (j,k) are the discrete pixel coordinates corresponding to image coordinates (x,y). $d_{j,k}$ is the blur parameter at (j,k) which represents the level of defocus there. $\overline{d}_{j,k}$, and κ can be obtained by convolving $d_{j,k}$ with a computational molecule derived from a molecule that is appropriate for the biharmonic operator. It can be shown that

$$\begin{aligned}\overline{d}_{j,k} = \frac{1}{20}[&8 \cdot (d_{j+1,k} + d_{j,k+1} + d_{j-1,k} + d_{j,k-1}) \\ &-2 \cdot (d_{j+1,k+1} + d_{j+1,k-1} + d_{j-1,k+1} + d_{j-1,k-1}) \\ &-(d_{j,k+2} + d_{j+2,k} + d_{j-2,k} + d_{j,k-2})]\end{aligned} \tag{20}$$

and $\kappa = 20$. The first term in Eq. 19 is $\frac{\partial}{\partial d_e}\mathcal{F}$, and it is estimated by a finite difference method. The discrete version of the Euler-Lagrange equation is

$$\frac{\partial}{\partial d_e}\sum_d (g_o - g_e)^2 + 2\lambda\kappa \cdot (d_{j,k} - \overline{d}_{j,k}) = 0 \tag{21}$$

This leads to an iterative formula of the form

$$d_{j,k}^{(n+1)} = \overline{d}_{j,k}^{n} - \frac{1}{2\lambda\kappa} \cdot \frac{\partial}{\partial d_e}\sum_d (g_o - g_e^n)^2 \tag{22}$$

Using this equation, the estimated solution of the 3D shape is updated iteratively.

3.1 Iterative Algorithm and Different Implementations

The following iterative algorithm was implemented for the regularization approach.

1. Record the observed image data $g_o(d, x, y)$ of a given 3D scene with focused image $F_o(x', y')$ and depth-map $u'_o(x', y')$. Let the FIS corresponding to this depth-map be $d_o(x', y')$.

2. Obtain an initial estimate of the solution for focused image and FIS by applying IFA and/or IDA to the observed image data. Let the estimated focused image be $F_e(x', y')$ and FIS be $d_e(x', y')$.

3. Update the initial solution iteratively using Eq. 22. In each iteration, the updated solution is checked for the depth and brightness positivity constraints and the local error-control constraint. If necessary, the solution is modified appropriately to satisfy the constraints.

4. Stop iterating when certain criterion is met (e.g. error stops decreasing or a certain maximum number of iterations has been completed).

It is necessary to select a good λ in order to attain a balance between the data similarity error (E_i) and smoothness of FIS (E_s). Depending on the initial solution, the derivative of the quadratic error term changes from point to point. Locally this variation may be small, but it can change substantially from one image region to another. This phenomenon makes the choice of the regularization parameter λ difficult. After a few trials, a value of 50 for λ was found to give satisfactory results. Further, the second term that gives the adjustment value at any iteration was limited to a magnitude of $0, \pm 1\epsilon, \pm 2\epsilon, \pm 3\epsilon$ where ϵ was the sampling interval (roughly equal to the size of one pixel) along the d dimension. In one variation of our algorithm the maximum adjustment value was taken to be 3ϵ in the first two iterations, 2ϵ in the next two iterations, and 1ϵ in the subsequent iterations. However there was no significant difference in its performance. The results of the regularization approach were compared with two other approaches explained next.

4 Gradient Descent and Local Search Methods

4.1 Gradient Descent Method

The solution for 3D shape and focused image was obtained by minimizing the sum of squared error (E_i) between the observed image data and the estimated image data. The focused image surface in a small image region (of about 8x8 size) is approximated by a piecewise planar surface patch with three parameters– slope with respect to x-axis, slope with respect to y-axis, and z-axis intercept. Error gradient with respect to these three parameters were used in the gradient descent error minimization. Three gradient descent type methods have been used in our research. In the first method, a search for the parameters that minimize the error is made by considering one parameter at a time. We call this the Sequential Parameter Search (SPS) method. In the second method, the parameter space is searched considering all parameters simultaneously. We call this the Parallel Parameter Search (PPS) method. In the third method, first SPS is applied and then PPS is applied. This is called the Sequential and Parallel Parameter Search (SPPS) method. These methods are based on the iterative gradient descent approach of going downhill with respect to the error function to find the lowest point. The initial solution for 3D shape is

obtained by a traditional IFA method. In each iteration, an improved estimate of the parameters is obtained by adjusting their values based on the error gradient. The iterative search for the parameters that minimize the error stops when the error stops decreasing. More details on SPS, PPS, and SPPS can be found in.[7]

4.2 Local Search Method

The local search method is an iterative error minimization method similar to a brute force search method. The difference is that this approach searches for the best 3D shape of FIS in a narrow range around the initial solution at each pixel. In our implementation, the initial solution is obtained from the SPS method. This solution is refined by adjusting the shape of FIS at each pixel by one unit at a time iteratively along the direction which decreases the error. The estimated 3D shape is continually updated until no further improvement is possible. This method provides a very accurate result but it needs a lot of computation.

5 Simulation and Experimental results

A $32 \times 32 \times 32$ size image volume data was synthesized where the FIS was a hemispherical object (with radius 24) and the focused image was a checker board (see Figs. 7,8) . Another similar but larger $64 \times 64 \times 32$ size image volume data was generated. From UFDA, the observed image data $g(i, j, k)$ was synthesized using Eq.(2) with camera parameters (D=9mm, f=35mm, s= 35mm to 36.5mm). Then an initial solution for the focused image and the estimated 3D shape was obtained using an IFA method. In the IFA method, a focus measure (energy of image Laplacian) was computed in 8×8 non-overlapping regions. A piecewise constant approximation to the focused image surface in each 8×8 image region was obtained by finding the position where the focus measure was a maximum. These estimated solutions and the 3D PSF were used to compute the estimated image data $g'(i, j, k)$ using Eq.(2). The error E_i between the observed image data $g(i, j, k)$ and the estimated image data $g'(i, j, k)$ was computed using Eq.(6). The regularization, gradient descent, and local search methods described earlier were applied to the image volume data.

The original focused image surface and focused image for the $32 \times 32 \times 32$ and $64 \times 64 \times 32$ image model are shown in Figs.(7,8,3) . The initial solution for these two images are shown in Figs.(9,10,4). The results from these three types of method are presented by the percentage error in gray level per pixel between the observed image and the images estimated from the best solutions for a $32 \times 32 \times 32$ image volume. A comparison of the computation time for each method are also shown in Fig.(11). The reconstructed 3D shape and focused image for the gradient descent approach are shown in Figs.(12,13); the results for local search method are shown in Figs. (14,15), and the results for the regularization method (7 iterations) are presented in Figs. (16,17). For $64 \times 64 \times 32$ image data, the results of the regularization method for 3 and 7 iterations are shown in Figs. (5,6).

6 Conclusion

The theory and application of a regularization approach to UFDA has been presented. Its performance has been compared with gradient descent methods and a local search method. In our experiments, the regularization approach performed better than other approaches in terms of accuracy and computational time. We recommend this approach for smooth objects in practical applications. One disadvantage of this approach is that it involves the selection of the regularization parameter λ. The gradient descent approach also performs well and is useful in the case of rough (non-smooth) objects for which the regularization approach is unsuitable. In particular, SPS offers a good balance between accuracy and computational time. The pixel-by-pixel search improves upon the accuracy of SPS at the cost of high computation.

Acknowledgement: The support of this research in part by the Olympus Optical Co. is gratefully acknowledged.

7 REFERENCES

[1] N.I. Akhiezer, *The Calculus of Variations,* Blaisdell Publishing Company, pp104-109, First Edition , 1962.

[2] J. Enns and P. Lawrence, "A Matrix Based Method for Determining Depth from Focus", *Proceedings of the IEEE Computer Society Conference on Computer Vision and Pattern Recognition*, June 1991.

[3] B. K. P. Horn, *Robot Vision,* McGraw-Hill Book Company, 1986.

[4] M. Subbarao, and M. C. Lu, "Computer Modeling and Simulation of Camera Defocus", *Machine Vision and Applications*, (1994) 7, pp. 277-289.

[5] M. Subbarao and G. Surya, "Depth from Defocus: A Spatial Domain Approach", *International Journal of Computer Vision*, 13, 3, pp. 271-294 (1994).

[6] M. Subbarao and T. S. Choi, "Accurate Recovery of Three-Dimensional Shape from Image Focus", *IEEE Transactions on Pattern Analysis and Machine Intelligence,* March 1995, pp. 266-274.

[7] M. Subbarao and Y.F. Liu, " Accurate Reconstruction of Three-dimensional shape and Focused Image from a Sequence of Noisy Defocused Images", SPIE Vol.2909 pp 178-191, Boston Mass. Nov. 1996

[8] T. Poggio, V. Torre, C. Koch " Computational vision and regularization theory", Nature, Vol.317,No.6053, pp314-319, Sep 1985

[9] Tikhonov, A.N. , Arsenin, V.Y. *Solutions of ill-posed Problems*, Winston, Washington, DC , 1977

[10] A. Rosenfeld and A. C. Kak, *Digital Picture Processing*, Vol. 1, Academic Press, 1982.

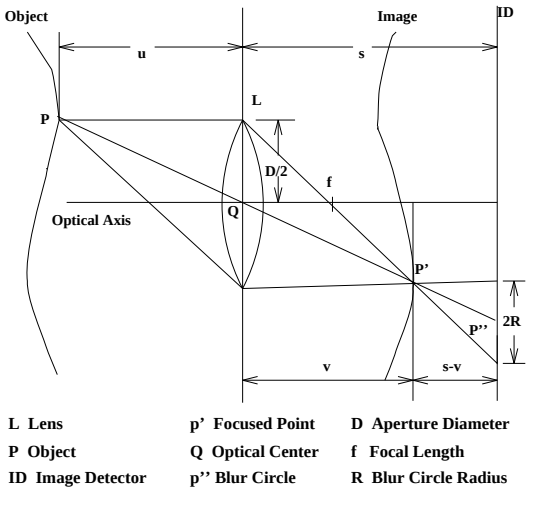

Figure 1: Image Formation Model

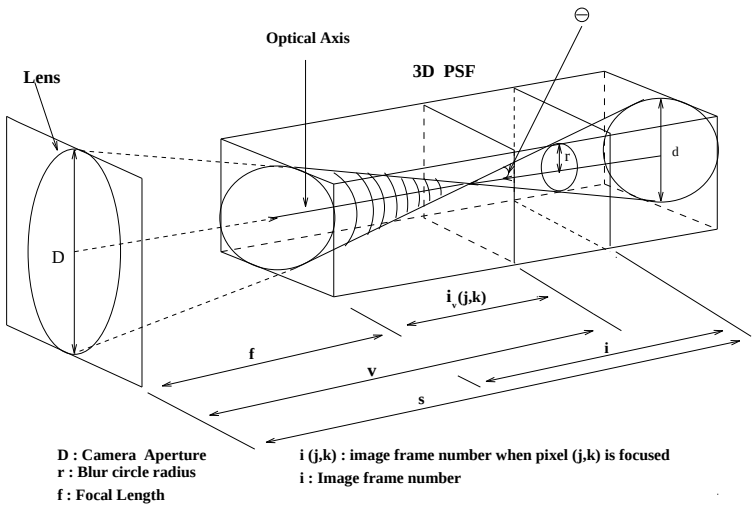

Figure 2: 3D PSF

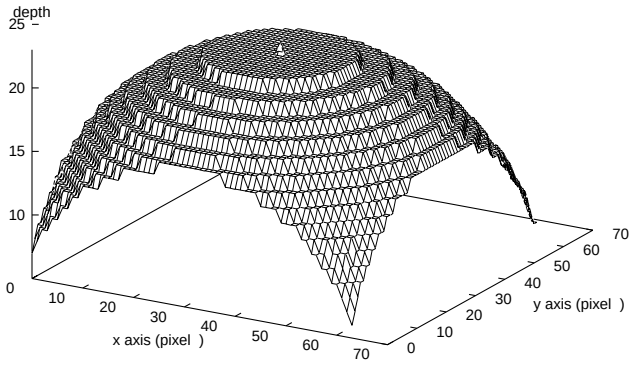

Figure 3: Orginal FIS of a 64x64 Hemisphere

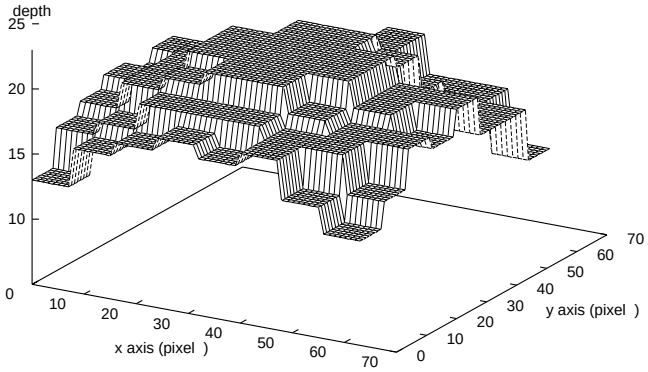

Figure 4: Initial solution for FIS

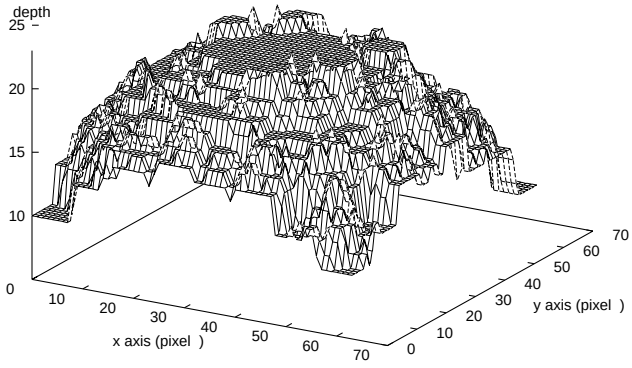

Figure 5: FIS recovered (3 iterations)

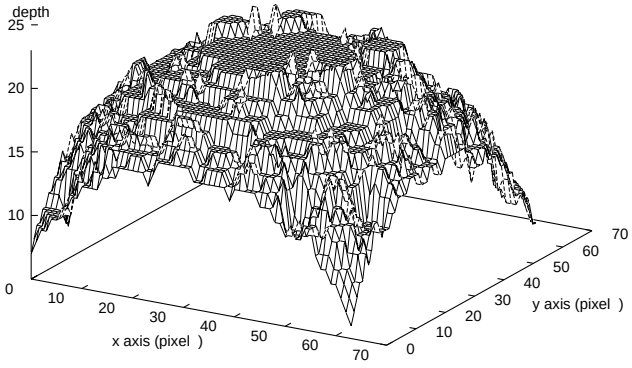

Figure 6: FIS recovered (7 iterations)

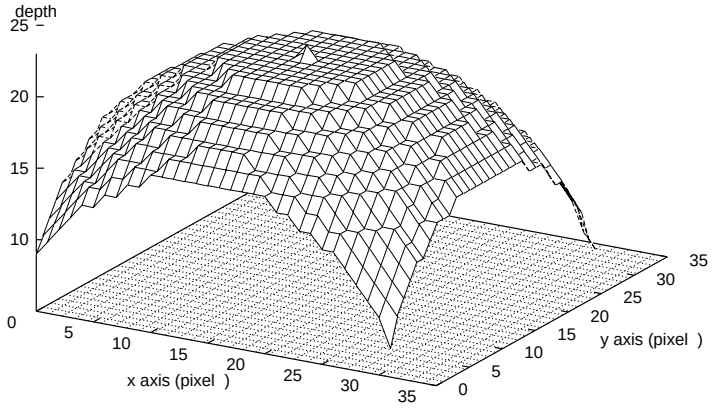

Figure 7: Original FIS of a 32x32 Hemisphere

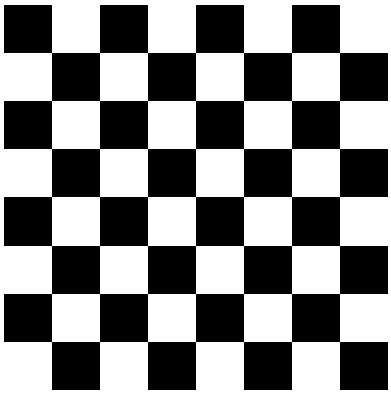

Figure 8: Original Focused Image

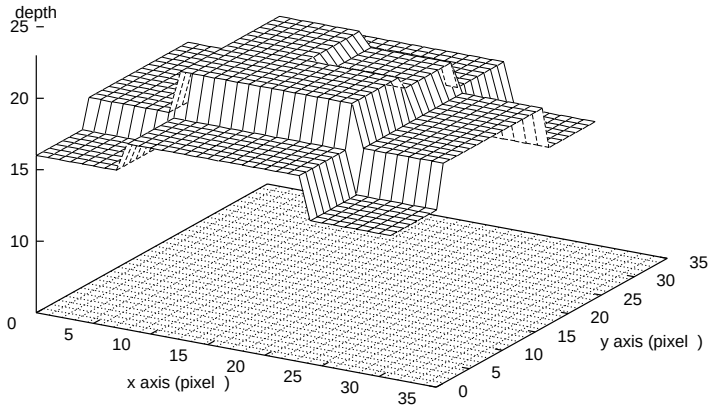

Figure 9: Initial Solution for FIS

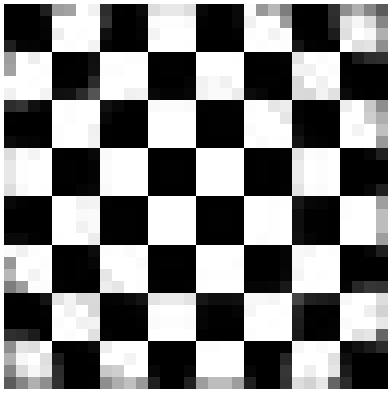

Figure 10: Initial solution for Focused Image

	SPS	PPS	SPPS	P_by_P	Regularization 7 iteration
% of gray level	5.25%	7.25 %	4.75 %	2.89 %	2.02 %
computation time (minute)	4	5	7	14	5

Figure 11: Comparison of different methods

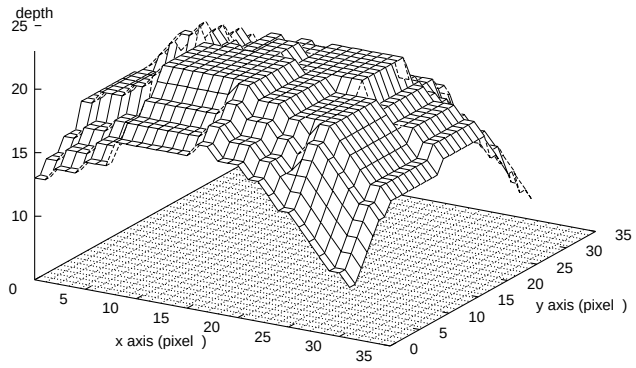

Figure 12: FIS by gradient descent method

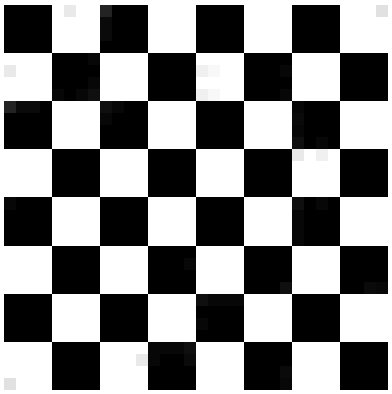

Figure 13: Focused Image by gradient descent method

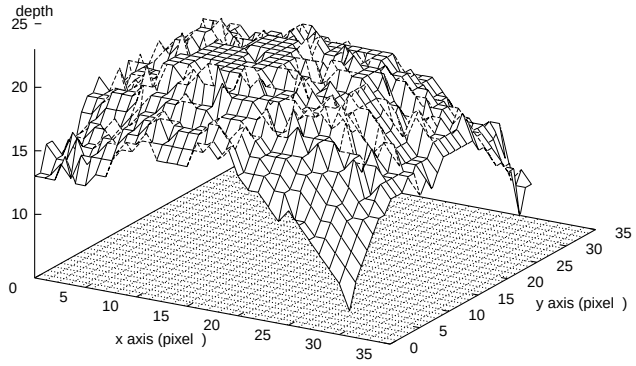

Figure 14: FIS by local search method

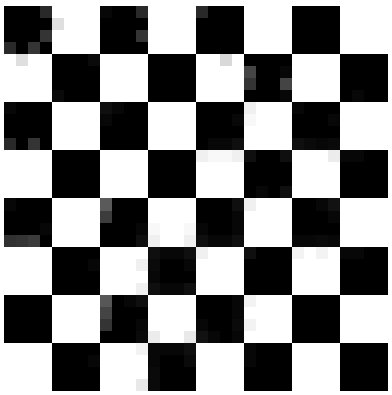

Figure 15: Focused Image by local search method

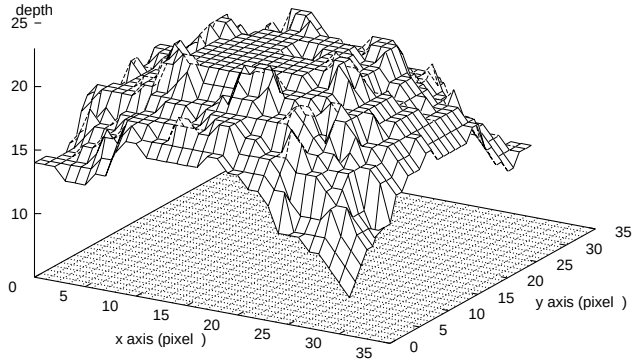

Figure 16: FIS by regularization (7 iters.)

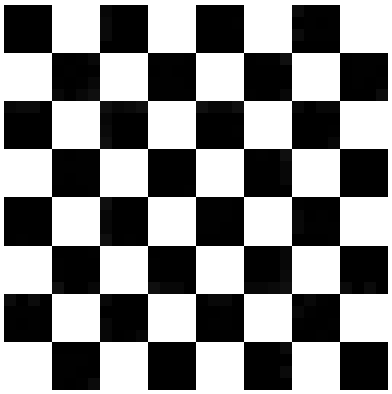

Figure 17: Focused Image by regularization (7 iters.)